

Loading of a cold atomic beam into a magnetic guide

P. Cren, C. F. Roos, A. Aclan, J. Dalibard and D. Guéry-Odelin

Laboratoire Kastler Brossel^a, Département de Physique de l'Ecole Normale Supérieure,
24 rue Lhomond, 75005 Paris, France

October 26, 2018

Abstract. We demonstrate experimentally the continuous and pulsed loading of a slow and cold atomic beam into a magnetic guide. The slow beam is produced using a vapor loaded laser trap, which ensures two-dimensional magneto-optical trapping, as well as cooling by a moving molasses along the third direction. It provides a continuous flux larger than 10^9 atoms/s with an adjustable mean velocity ranging from 0.3 to 3 m/s, and with longitudinal and transverse temperatures smaller than $100 \mu\text{K}$. Up to $3 \cdot 10^8$ atoms/s are injected into the magnetic guide and subsequently guided over a distance of 40 cm.

PACS. 32.80.Pj, 42.50.Vk, 03.75.Be

1 Introduction

A large variety of techniques based on the use of electromagnetic forces are now available to control the motion of atoms [1, 2, 3] and molecules [4, 5, 6, 7]. The progress in this domain has opened the way to several fields of applications such as atom optics and interferometry [8], precision experiments and metrology [9], and statistical physics, with the achievement of degenerate Bose or Fermi gases [10]. Among these techniques, a special effort has been devoted to the production of slow and cold continuous atomic and molecular beams, since they represent a powerful tool for many of the above mentioned applications.

A spectacular challenge in this field consists in the achievement of a continuous beam operating in the quantum degenerate regime. This would be the matter wave equivalent of a cw monochromatic laser and it would allow for unprecedented performances in terms of focalization or collimation. A possible way to achieve this goal has been studied theoretically in [11]. In this proposal, a non-degenerate, but already slow and cold beam of particles, is injected into a magnetic guide [12, 13, 14, 15, 16, 17, 18, 19] where transverse evaporation takes place. If the elastic collision rate is large enough, efficient evaporative cooling will lead to quantum degeneracy after a propagation length in the guide compatible with experimental constraints (*i.e.* a few meters). Therefore the success of this project relies upon two preliminary and separate accomplishments. First, one has to build a source of cold atoms as intense as possible, and secondly, one has then to inject the atoms into a magnetic guide, where they should propagate with reduced losses over a long distance.

When resonant laser light is available at the atomic resonance frequency, a convenient method for producing a bright source of slow atoms consists in decelerating a thermal beam with radiation pressure [20, 21], and subsequently applying transverse cooling and trapping to the slow atomic beam (“atom funnel”) [22, 23, 24, 25, 26]. Alternatively, one can extract a jet of atoms from a vapor-loaded magneto-optical trap (MOT). The simplest scheme consists in a 2D MOT [27, 28] where the MOT laser beams propagate only in the xy plane, resulting in a uncooled atom jet along the z axis. As for some of the demonstrated funnels [22, 24, 26], one can narrow the longitudinal velocity distribution, using a moving molasses scheme, *i.e.*, a pair of counter-propagating laser beams along the atomic beam axis, with two different frequencies [29]. The atoms are then bunched in a non-zero velocity class, which corresponds to the moving frame where both lasers are seen with equal frequencies. One can also produce a beam with two or more velocity components using a 2D (xy) magneto-optical trap and a static magnetic field superimposed with a static optical molasses along the beam axis (z) [29, 30, 31]. Alternatively a collimated beam of atoms can be obtained by drilling a hole in one of the mirrors used for the MOT [32] (see also [27]), with a pyramidal mirror structure with a hole at its vertex [33, 34, 35], or with an extra pushing beam, which destabilizes the MOT at its center [36, 37]. All these sources produce a relatively bright beam (from 10^6 to several 10^{10} atoms per second), with an average velocity \bar{v} between 1 and 50 m/s; for most of them the velocity distribution is rather broad, with a dispersion $\Delta v \sim \bar{v}$.

In the perspective of loading a magnetic guide in order to perform evaporative cooling, the atom source should provide an average velocity \bar{v} smaller than 2 m/s, and it should be as cold as possible, both longitudinally and

^a Unité de Recherche de l'Ecole Normale Supérieure et de l'Université Pierre et Marie Curie, associée au CNRS.

transversally ($\Delta v \ll \bar{v}$). This eliminates most of the source types described above, in particular those from the “leaking MOT” family, and also the sources producing a beam with multiple velocity components. One is then left with the principle of a source which uses a moving molasses (MM) on axis, together with a transverse magneto-optical trap (MOT), which we shall designate in the following as a “MM-MOT”.

In the present paper, we describe in § 2 our vapor loaded MM-MOT, which produces a very slow and cold atomic beam (\bar{v} between 0.3 and 3 m/s, $\Delta v < \bar{v}/10$), and which is well suited for loading a magnetic guide, either continuously or in a pulsed manner. We also compare our results with previously reported work. In § 3, we show how to inject this atomic beam into a magnetic guide, created by a quadrupole field in the xy plane. We discuss in the concluding section (§ 4) the perspectives opened by this experimental setup for the development of a continuous, evaporatively cooled, atomic beam. The present performances of our system are still far from the requirements for initiating forced evaporative cooling in the magnetic guide. However, with an improved setup, we hope to reach the desired conditions as discussed in the concluding section.

2 The “MM - MOT”

In this section we describe the principle and the practical realization of the MM-MOT, whose purpose is to provide a cooling along the z axis, in the moving frame defined by the moving molasses (MM), and a magneto-optical trapping (MOT) in the xy plane. This setup is employed to capture ^{87}Rb atoms from the background gas.

2.1 Principle of the MM-MOT

The MM-MOT is based upon a four-beam laser configuration similar to the one used for the study of optical lattices described in [38], superimposed with a linear magnetic 2D quadrupole field.

The magnetic quadrupole field is created by four rectangular, elongated coils located in the planes $x = \pm 8$ cm and $y = \pm 8$ cm. The currents in the coils facing each other have opposite sign so that, close to the symmetry axis $x = y = 0$, the resulting field is given by

$$\mathbf{B} = (-b'x, b'y, 0).$$

The field is zero along the z axis and the transverse gradient is typically $b' = 0.1$ T/m.

The optical arrangement consists of four laser beams in a tetrahedral configuration (see Fig. 1). Two laser beams with frequency ω propagate in the yz plane along the directions $\cos \alpha \mathbf{u}_z \pm \sin \alpha \mathbf{u}_y$, with a positive helicity. The two other beams with frequency ω' propagate in the xz plane along the directions $-\cos \alpha \mathbf{u}_z \pm \sin \alpha \mathbf{u}_x$, with a negative helicity. The four beams are red-detuned with respect to the atomic transition

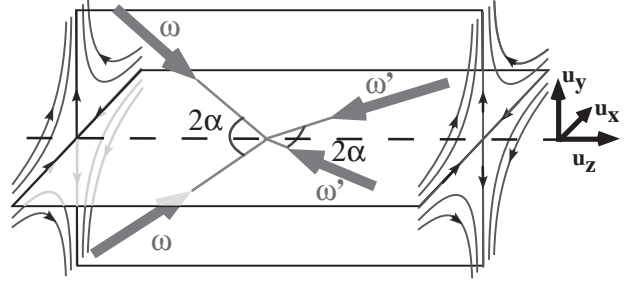


Fig. 1. Laser configuration of the 2D MOT

$|5S_{1/2}, F = 2\rangle \rightarrow |5P_{3/2}, F = 3\rangle$, whose frequency is called ω_a . The average detuning $\delta = \bar{\omega} - \omega_a$, with $\bar{\omega} = (\omega + \omega')/2$, is typically -3Γ , where $\Gamma = 2\pi \times 5.9$ MHz denotes the natural width of the excited level of the transition.

For $\alpha = \pi/2$ and $\omega = \omega'$, one obtains the “standard” 2D-MOT configuration [27], that confines and cools the atoms transversally without affecting the longitudinal motion. For $\alpha \sim \pi/4$, one obtains an efficient cooling of the atomic motion along the z direction, while still keeping an efficient magneto-optical trapping in the xy plane. In our experiment we work with $\alpha = 47^\circ$.

Because of the frequency difference $\omega - \omega'$ between the two pairs of beams, the cooling corresponds to an accumulation of the atoms around the velocity class

$$\bar{v} = \frac{\omega - \omega'}{2k \cos \alpha}, \quad (1)$$

where k is the wave vector of the laser light. By scanning $\omega - \omega'$ between 0 and $2\pi \times 5$ MHz (*i.e.* a small fraction of the detuning δ), one can adjust the mean velocity \bar{v} between 0 and ~ 3 m/s.

We have confirmed this qualitative understanding of the MM-MOT using a numerical integration of the trajectories of the atoms in the corresponding laser configuration. This treatment follows the same lines as in [36]. We model the atomic transition as a $|g, J_g = 0\rangle \leftrightarrow |e, J_e = 1\rangle$ transition with frequency $\hbar\omega_a$, where $|g\rangle$ and $|e\rangle$ stand for the ground and excited state respectively. We denote by $I_{\text{sat}} = 16.2 \text{ Wm}^{-2}$ the saturation intensity for this transition. For each of the laser beams ($j = 1, \dots, 4$) and for each of the transitions $|g\rangle \leftrightarrow |e_m\rangle$ ($m = -1, 0, 1$), we introduce the position and velocity dependent saturation parameter

$$s_{j,m} = \frac{I_{j,m}}{I_{\text{sat}}} \frac{\Gamma^2}{\Gamma^2 + 4(\delta_j - \mathbf{k}_j \cdot \mathbf{v} + m\mu B/\hbar)^2}.$$

Here μ is the magnetic moment associated with the level $|e\rangle$, B is the local magnetic field amplitude, and \mathbf{k}_j , δ_j and $I_{j,m}$ denote the wave vector, detuning and local intensity of the j -th laser wave, driving the $|g\rangle \leftrightarrow |e_m\rangle$ transition. We then choose the following approximate expression for the total radiative force acting on an atom:

$$\mathbf{F} = \sum_i \hbar \mathbf{k}_i \frac{\Gamma}{2} \frac{\sum_m s_{i,m}}{1 + \sum_{j,m} s_{j,m}}. \quad (2)$$

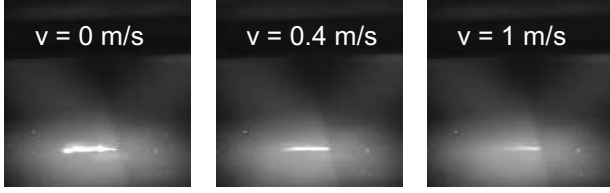


Fig. 2. Photograph of the 2D MOT for various mean velocities. From left to right: $\bar{v} = 0, 40, 100$ cm/s.

A detailed discussion of the approximations leading to (2) can be found in [36]. Here we simply recall that this expression corresponds to the spatial average of the radiative force over a cell of size $\lambda^3 = (2\pi/k)^3$, so that all interference terms varying as $i(\mathbf{k}_j - \mathbf{k}_{j'}) \cdot \mathbf{r}$ have been neglected.

In the simulation the initial position of each atom is chosen following a uniform spatial distribution on the walls of the vacuum vessel. The initial velocity is given by the Maxwell Boltzmann distribution for $T = 300$ K. By computing a large number of trajectories, one obtains the probability for an atom to be captured and transferred into the jet, as well as the jet characteristics which are the velocity distribution, the divergence, and the total flux. The total flux of the simulated jet is calculated using the real number of atoms \dot{N} emitted per unit time and per unit surface of the cell at a pressure P . One obtains $\dot{N} = P/\sqrt{2\pi m k_B T}$ [39]. Note that the simulation neglects interaction effects like collisions and multiple light scattering. The validity of the linear scaling with pressure is limited to the low pressure regime ($P < 10^{-7}$ mbar) where the characteristic time of ~ 20 ms for extracting an atom out of the MM-MOT is shorter than the collision time.

In addition to confirming the qualitative understanding of the MM-MOT, this simulation is particularly helpful for optimizing certain parameters for which a fine tuning on the real experimental setup would be tiresome. In particular we used it for the determination of the optimal laser waists for the experimentally available laser power.

2.2 Experimental realization of the MM-MOT

The trap is created in a rectangular glass cell ($130 \text{ mm} \times 50 \text{ mm} \times 50 \text{ mm}$) and the atoms are captured from the low-pressure background gas. The partial pressure for ^{87}Rb is measured by the absorption of a resonant beam. It can be varied from 10^{-9} mbar up to the saturated vapor pressure at room temperature (3×10^{-7} mbar) by controlling the temperature of the Rb-reservoir or the aperture of the intermediate valve.

The laser light for the magneto-optical trap originates from four laser diodes (one per beam), which are injection-locked to a master diode. Each trapping beam has a circular beam profile with a waist of about 15 mm and a power of 30 mW at the level of the trap. The linewidth of the master diode is narrowed by optical feedback from an external grating. It is split into two beams, each of which passes through an acousto-optic modulator, which provides the frequencies ω and ω' . The stability of $\omega - \omega'$ is

better than 10 kHz, which defines the velocity \bar{v} to better than 0.5 cm/s.

A second grating stabilized laser diode, resonant with $|5S_{1/2}, F = 1\rangle \rightarrow |5P_{3/2}, F = 2\rangle$, illuminates the MM-MOT. This repumping laser prevents the accumulation of atoms in the ground level $F = 1$ by optical pumping. Both master lasers are frequency stabilized using saturated absorption spectroscopy in a rubidium vapor cell.

Photographs of the fluorescence light emitted by the trapped atoms are shown in Fig. 2 for various mean velocities \bar{v} . We observe elongated clouds of atoms with a length $L \sim 20$ mm and a transverse size $\sim 500 \mu\text{m}$. Due to local imperfections of the intensity profile of the laser beams, the atomic cloud does not have a straight shape over its whole length when it is at rest ($\omega = \omega'$). One rather observes a wiggling line with an amplitude $\sim 500 \mu\text{m}$ (Fig. 2a). These wiggles disappear as soon as one imposes a non-zero mean velocity \bar{v} on the atoms (Fig. 2b,c).

2.3 Characterization of the MM-MOT

The characterization of this trap consists in determining the main features of the atomic beam that is produced: mean velocity, longitudinal and transverse temperatures, and flux. The first quantities are determined from the absorption of a probe beam located at a distance z_0 away from the output of the MM-MOT, while the latter is inferred from the fluorescence light emitted by the atoms in the trap region.

2.3.1 Longitudinal velocity distribution

In order to investigate the velocity distribution of the atomic beam along the z axis, we use a time-of-flight technique. We operate the MM-MOT with a plug laser beam present which blocks the outgoing atomic beam by pushing the atoms away from the z axis. At time $t = 0$, we switch off the plug beam, so that the atomic beam can propagate freely and we monitor as a function of time the modification of the absorption of a probe beam located further downstream.

The probe beam is tuned to the $|5S_{1/2}, F = 2\rangle \rightarrow |5P_{3/2}, F = 3\rangle$ transition, superimposed with a weak repumping laser to overcome optical pumping effects. The waist of the probe beam is $160 \mu\text{m}$ and its distance z_0 from the end of the MM-MOT is 8.3 mm. This distance is large in comparison with the diameters of the plug and probe beams and has been chosen in order to overcome spatial size effects.

The absorption of the probe beam is detected by a photodiode. A typical step-shaped signal is given in Fig. 3. The solid curve is a fit from the relation

$$s(z_0, t) \propto 1 - \text{Erf}\left(\frac{z_0 - \bar{v}t}{\sqrt{2}\Delta v_{\parallel}t}\right), \quad (3)$$

which corresponds to the expected time-of-flight signal assuming a Gaussian velocity distribution centered on \bar{v}

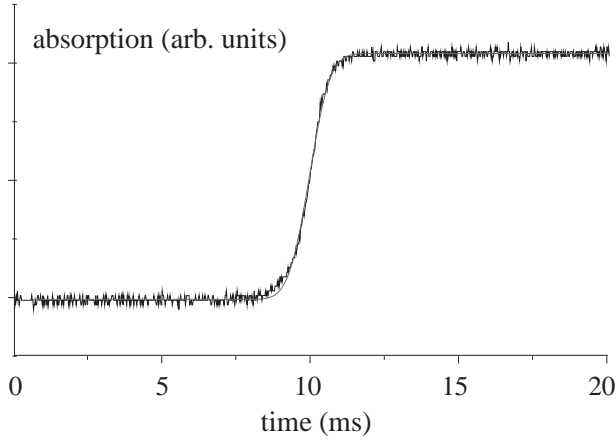


Fig. 3. Time of flight signal from the MM-MOT. The straight line is a fit using (3) with $\bar{v} = 84$ cm/s and $\Delta v_{\parallel} = 4.6$ cm/s.

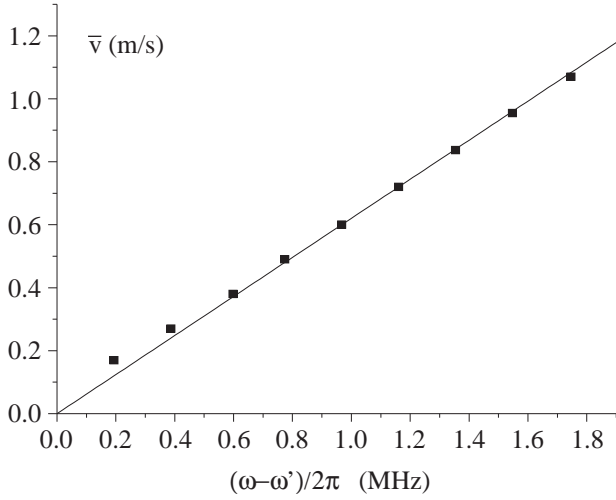


Fig. 4. Mean velocity \bar{v} of the beam as a function of the frequency difference $\omega - \omega'$.

and with a dispersion Δv_{\parallel} . We find generally an excellent agreement between this fitting function and the experimental signal. For the particular case of Fig. 3, we obtain $\bar{v} = 84$ cm/s and $\Delta v_{\parallel} = 4.6$ cm/s, corresponding to a longitudinal temperature $T_{\parallel} = m \Delta v_{\parallel}^2 / k_B = 23$ μ K.

Fig. 4 shows the measured mean velocity of atoms along the z axis as a function of the frequency difference $\omega - \omega'$ between the two pairs of trapping beams. As expected from (1), we find a linear relation with a slope in agreement with the imposed geometry ($\alpha = 47^\circ$).

We have measured the longitudinal temperature T_{\parallel} as a function of the mean velocity. The results are shown in Fig. 5. The longitudinal temperature increases when the mean velocity increases. The atomic beam which is produced in this experiment is quasi mono-kinetic. We find that $\Delta v_{\parallel} / \bar{v} < 0.1$ over the whole range 0.3–3 m/s for \bar{v} . The lowest temperature $T_{\parallel} = 10$ μ K is obtained for $\bar{v} = 60$ cm/s.

This temperature is significantly smaller than what is expected from standard laser cooling theory, for our trap-

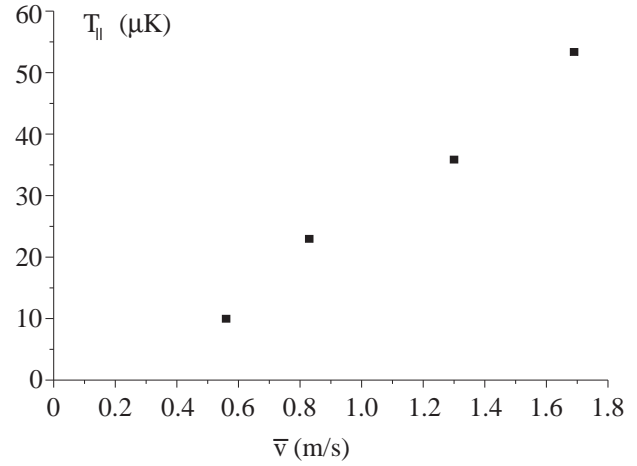


Fig. 5. Longitudinal temperature T_{\parallel} as a function of the mean velocity \bar{v} of the beam.

ping beam intensity and detuning. Such a low temperature probably results from an additional cooling of the atoms as they slowly move out from the trapping beams. A similar effect occurs for 3D-MOT in the time domain, when one switches relatively slowly the MOT beams (see [40, 41]). In the context of slow atomic beams generated from a MOT, it has also been observed in [26].

2.3.2 Transverse temperature of the beam

The geometry of the MM-MOT creates a strong asymmetry between the longitudinal z axis and the transverse xy axes. For $\alpha \sim 0$, the cooling is much more efficient along the z axis than in the xy plane, and the conclusion is reversed when $\alpha \sim \pi/2$. Therefore there is no reason to expect that the two velocity distributions are characterized by the same temperature, unless the elastic collision rate is large enough to thermalize all degrees of freedom of the atomic beam. However, the spatial densities achieved so far in our experiment are too low for this thermalization to occur when the atoms travel over the distance z_0 .

We have measured directly the transverse size of the atomic beam by scanning the probe beam position. In this way, we deduce an upper bound for the transverse temperature. We find $T_{\perp} = 35$ μ K for $\bar{v} = 0.3$ m/s and $T_{\perp} = 80$ μ K for $\bar{v} = 1$ m/s. Again, this variation of the temperature with the longitudinal velocity can be attributed to the extra cooling which occurs when the atoms leave the trapping region slowly enough.

2.3.3 Loading and steady-state flux of the atomic source

The loading dynamics of the MM-MOT can be understood with a simple model based on the fact that even for the highest average velocities \bar{v} we have produced ($\bar{v} = 3$ m/s), the average time $L/(2\bar{v})$ required for an atom to leave the MM-MOT ($L \sim 2$ cm is the length of the atomic cloud) is larger than the transverse trapping time deduced from

our simulation (~ 2 ms). Therefore we can assume that the loading rate R of the MM-MOT (number of atoms captured per unit length and unit time) is independent of the velocity \bar{v} , for the velocity range considered here. Consider now a point inside the MM-MOT close to the trap exit. The time dependence of the linear density in this point is expected to vary as

$$n(t) = R \int_0^{\min(t, L/\bar{v})} e^{-\gamma t'} dt', \quad (4)$$

where γ denotes the loss rate of atoms from the trap, *e.g.* due to collisions with the residual gas. In particular, the steady state value of this quantity is $n(\infty) = R/\gamma(1 - \exp(-\gamma L/\bar{v})) \simeq RL/\bar{v}$ if the lifetime γ^{-1} is much larger than the “launching time” L/\bar{v} . This corresponds to a steady-state atom flux $\Phi = RL$ independent of the mean velocity \bar{v} .

The measurement of the linear density of trapped atoms confirms this simple model, as can be seen in Fig. 6. This measurement is performed by analyzing the fluorescence signal emitted from a small region located close to the trap exit. In order to avoid difficulties related with a residual magnetic field or with inhomogeneities in the laser beam profiles, we calibrate the fluorescence measurement by suddenly bringing the trapping laser frequency in resonance with the atoms, so that each atom emits $\sim \Gamma/2$ photons/s for a short time before being expelled.

The linear increase of the signal at short times shown in Fig. 6a is the same for all velocity classes and it gives $R \simeq 10^9$ atoms/s/cm for a ^{87}Rb rubidium vapor pressure $P_{87} = 3 \cdot 10^{-9}$ mbar. For long loading times, the linear density $n(t)$ saturates to a value $n(\infty)$ which is approximately proportional to $1/\bar{v}$ (Fig. 6b). This shows that the steady state flux $\Phi = \bar{v} n(\infty)$ is independent of the average velocity of the beam, as predicted by the simple model described above. This flux is proportional to P_{87} in the range 10^{-9} mbar $< P_{87} < 10^{-8}$ mbar, and we obtain:

$$\Phi = 10^9 \text{ atoms/s for } P_{87} = 10^{-8} \text{ mbar.}$$

The measured flux is in good agreement with the predictions of the simulation described in §2.1. For the same laser intensities and waists, the simulation gives after averaging over the atomic trajectories a capture velocity $v_{\text{cap}} = 34$ m/s, corresponding to a flux $\Phi = 2.2 \cdot 10^9$ atoms/s for $P_{87} = 10^{-8}$ mbar. Since $\Phi \propto v_{\text{cap}}^4$, this means that the simulation overestimates the capture velocity by 20%. This slight probably results from the approximations which led to the expression (2) for the radiative force in the MM-MOT.

2.4 Comparison with previous works

As already mentioned in the introduction, our experimental setup for the MM-MOT is quite different from the devices of the leaking MOT family. These devices all lead to an average velocity which is at least one order of magnitude larger than the lowest velocity demonstrated here,

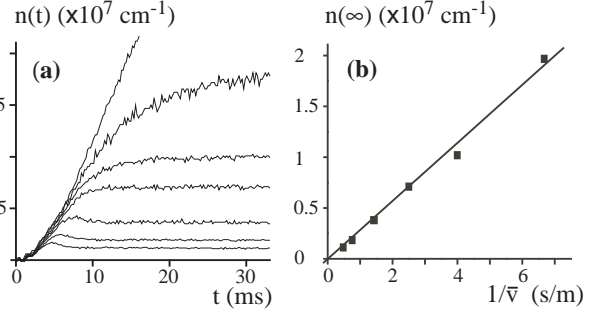


Fig. 6. (a) Time variation of the linear density $n(t)$ at the exit of the MM-MOT, inferred from the fluorescence intensity at this location, for various launching velocities \bar{v} (from top to bottom, $\bar{v} = 0, 15, 25, 40, 70, 130, 210$ cm/s). (b) Asymptotic linear density $n(\infty)$ as a function of the launching velocity \bar{v} .

and they could not be used as a convenient source for the magnetic guide in which we want to perform evaporative cooling. Our source presents certain similarities with the ones discussed in [24, 26, 29]. In these experiments, a magnetic configuration similar to ours was used and a moving molasses was produced along the beam axis, while two-dimensional magneto-optical trapping confined the atoms transversally. However, some important differences should also be pointed out between these experiments and our setup.

(i) The two experiments [24, 26] dealt with a decelerated atomic beam while our MM-MOT is directly loaded from the residual rubidium vapor pressure in our vacuum cell. This is an important simplification for our setup, yet there are some drawbacks. Since our purpose is to load a magnetic guide, we have to maintain a vacuum which is good enough to prevent collisional loss of atoms while they travel from the MM-MOT to the entrance of the magnetic guide. Typically we have to restrict the ^{87}Rb pressure to a value below 10^{-8} mbar, for an atom transit time of the order of 0.1 s. For this background pressure, our flux is respectively 6 times smaller and 2 times larger than what is reported in [24] and [26]. The experiment described in [29] was based on a vapor loaded trap as ours, but the reported flux was three orders of magnitude lower than the present one, which makes the design of [29] quite impracticable for our purpose.

(ii) We use a laser configuration with only four beams, instead of six. This is known as a very robust configuration for laser cooling and trapping processes. Any phase fluctuation of the laser beams only results in a translation of the whole interference pattern of the trapping beams [38], whereas in a five-beam or a six-beam configuration, this pattern changes when one of the phases of the beams fluctuates giving rise to heating. So far, we do not benefit from this increased stability, but it may play a role in future work. (iii) Finally we note that we have been able to operate our MM-MOT with exit velocities \bar{v} notably smaller than what is reported in [24, 26, 29] where $\bar{v} \geq 2$ m/s. This is important for the future implementation of forced evaporative cooling along the magnetic

guide into which the atomic beam is injected. For a given length of the guide, a smaller velocity leads to an increased evaporation time, and therefore a better cooling.

3 Loading of the magnetic guide

As explained in § 1, the second important result of the present paper concerns the injection of the slow atomic beam described above into a magnetic guide. This is an essential step towards the long term goal of this work, which consists in cooling the guided atoms by radio-frequency evaporation.

3.1 Characteristics of the guide

The magnetic guide has a total length of 60 cm. It is made out of four copper tubes ($\mathcal{O}_{\text{ext}} = 6$ mm and $\mathcal{O}_{\text{int}} = 4$ mm) placed in quadrupole configuration (see Fig. 7a). The tubes are located in the domain $z > 0$ and they are joined in $z = 0$ by a hollow metal cylinder, which allows for the circulation of current and cooling water from tube to tube. The axes of the copper tubes are placed at coordinates $x = \pm a; y = \pm a$, with $a = 7$ mm. A current $I = 400$ A can be sent through the tubes, which provides, far from the entrance of the guide (*i.e.* $z \gg a$), a magnetic gradient $b' = 3.2$ T/m in the xy plane.

The value of b' as a function of z is plotted on Fig. 7b. It changes sign in $z = -3$ mm and its absolute value is reduced by a factor larger than 100 for $z = -25$ mm, where the exit of the MM-MOT is located. Therefore this magnetic gradient does not affect the operation of the MM-MOT.

It is possible to superimpose a bias field parallel with the z axis to prevent Majorana spin flips when a guided atom passes close to the axis of the trap $x = y = 0$, where the trapping field is zero. In practice we have found that this bias field does not play a significant role, which can be easily understood by the following estimate. The probability for a spin flip when an atom passes close to the trap axis is $p \sim 2e^{-\xi}$, where $\xi = \pi\mu_B b' \rho^2 / (4\hbar v_{\perp})$ [42, 43]. Here ρ is the minimal distance from the z axis (*i.e.* the impact parameter), v_{\perp} designates the velocity in the xy plane at this location, and we assume that the atoms are trapped in the hyperfine state $F = 1, m = -1$, whose magnetic moment μ is half the Bohr magneton μ_B . Taking as a typical value $v_{\perp} \sim 0.1$ m/s, we find that p is important only if $\rho \leq 1$ μm . Therefore this loss term is not expected to play a role in our experiment, since the average impact parameter is ≥ 100 μm and the elastic collision rate is negligible. On the contrary, for higher atomic densities, elastic collisions can reload the phase space cells corresponding to trajectories with very small impact parameters. These losses should then play an important role, especially in our 2D quadrupole field where they occur close to a line, by contrast with a 3D quadrupole trap where they occur only around the central point. The presence of a bias field should then be crucial.

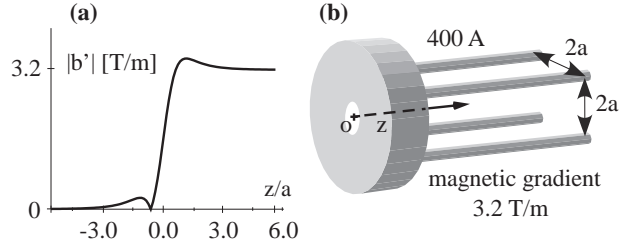


Fig. 7. Entrance of the magnetic guide. (a) Variation of the magnetic gradient in the xy plane as a function of z . (b) Schematic drawing of the guide. The cylindrical part located in close to $z = 0$ allows for the connection of the electrical currents and the water cooling circuit circulating into the four copper tubes.

A narrow glass tube ($\mathcal{O}4$ mm, length 170 mm) is centered at the entrance of the magnetic guide and aligned with the z axis. It ensures differential pumping between the MM-MOT cell, where the Rb partial pressure must be large enough to provide an efficient loading, and the chamber of the magnetic guide, where the residual pressure has to be minimized to avoid losses due to collisions with the background gas. We estimate that the pressure in this chamber is $\sim 4 \cdot 10^{-10}$ mbar, which corresponds to a lifetime ~ 20 s for the magnetically guided atoms.

3.2 Connection of the MM-MOT to the guide in continuous mode

The simplest way to load atoms from the MM-MOT into the guide consists in operating the MM-MOT continuously at a fixed velocity \bar{v} . As explained in § 2, the angle of the MM-MOT beams with the z axis is $\sim \pi/4$. Due to the presence of the metal cylinder located at the entrance of the magnetic guide (see Fig. 7a), the shortest distance between the output of the MM-MOT and the entrance of the magnetic guide is $D \sim 25$ mm. In other words, the MM-MOT is located in the region -45 mm $< z < -25$ mm and the atoms have to travel over a distance of 25 mm before being captured by the magnetic guide if they are in a magnetic sublevel corresponding to a low-field seeking state.

3.2.1 Free flight transfer

The simplest connection mode relies on ballistic flight to ensure the transfer between the MM-MOT and the magnetic guide. We place a laser tuned to the $|5S_{1/2}, F = 2\rangle \rightarrow |5P_{3/2}, F = 2\rangle$ transition in the region -25 mm $< z < 0$. The repumping laser is blocked in the transfer region, so that this extra “depumping” laser beam optically pumps the atoms in the $F = 1$ ground state. Therefore, provided that the three magnetic levels $m = 0, \pm 1$ of the $|5S_{1/2}, F = 1\rangle$ are equally populated, we expect that one third of the atoms (state $m = -1$) emerging from the MM-MOT can be captured by the magnetic guide. This

method based on ballistic flight is in principle quite simple, but has several drawbacks:

- It is restricted to relatively large velocities $\bar{v} > 1.5$ m/s. Otherwise the free-fall due to gravity, $gD^2/(2\bar{v}^2)$, is so large that the coupling to the guide becomes velocity-dependent.
- During the free flight, the atom jet spreads transversally, which leads to a strong increase of the transverse temperature in the guide, as compared with the MM-MOT. Consider for instance a beam emerging from the MM-MOT with $\bar{v} = 2$ m/s and $T_{\perp} = 100$ μ K. At the entrance of the magnetic guide, the radius of the beam is $R = (D/\bar{v})\sqrt{k_B T/M} \sim 1.2$ mm (M is the atomic mass). The corresponding magnetic energy is

$$E_{\text{mag}} = \mu b' R = (D\mu b'/\bar{v})\sqrt{k_B T/M}. \quad (5)$$

This gives $E_{\text{mag}}/k_B \sim 1$ mK in the present case.

- The optical pumping of the atoms to the hyperfine level $F = 1$ is not total, because of the stray light present at the repumping frequency $|5S_{1/2}, F = 1\rangle \rightarrow |5P_{3/2}, F = 2\rangle$. Therefore, after leaving the MM-MOT, the atoms may still be deflected by the residual radiation pressure force resulting from an imbalance between the intensities of the various laser beams. Although we took a particular care for adjusting the spatial profiles of these laser beams along the path corresponding to the trap exit, we found that it is very difficult to transfer slow atoms ($\bar{v} < 2$ m/s) with this method.

3.2.2 Use of an auxiliary transfer MOT

The difficulties mentioned above can be circumvented if we place an auxiliary guiding trap in the region -25 mm $< z < 0$. This trap is a pure 2D MOT, whose beams which are orthogonal to the z axis illuminate points up to 4 mm to the entrance of the magnetic guide (see Fig. 8). The transverse extension of the atomic beam at the entrance of the magnetic guide is then drastically reduced. As for the free flight transfer, we place a depumping laser at the entrance of the guide. The atoms are then trapped in the magnetic sublevel $J = 1, m = -1$, for which the amount of resonant stray light is too low to be an appreciable source of losses in the guide.

The disadvantage of this auxiliary trap concerns the broadening of the longitudinal velocity distribution, due to the random recoils associated with the spontaneous emission of photons as the atoms cross this auxiliary trap. However, as we show below (§ 3.4), this longitudinal heating remains relatively weak for a large detuning δ_2 of the auxiliary MOT. An upper limit for $|\delta_2|$ is given only by the condition that the radiative force of the auxiliary MOT has to overcome the spurious radiation pressure imbalance which exists in the wings of the MM-MOT lasers, as discussed above.

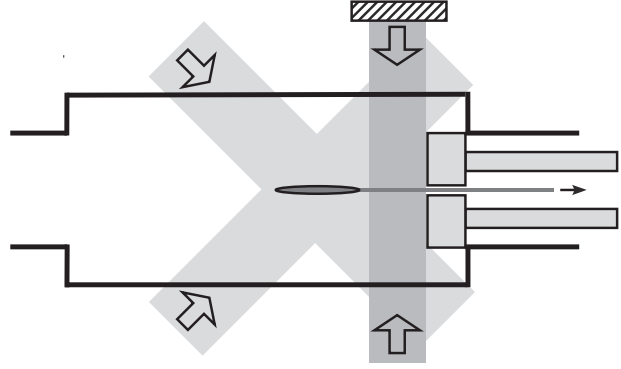


Fig. 8. Use of an auxiliary 2D MOT to transfer efficiently the atoms from the MM-MOT to the magnetic guide.

3.3 Connection of the MM-MOT to the guide in pulsed mode

The operation of the MM-MOT in a continuous mode, as described in the previous section (§ 3.2), imposes to search for a compromise between two different requirements. For an efficient loading one has to take a relatively small detuning ($\delta \sim -3\Gamma$), so that the trapping force is large. On the contrary, in order to minimize the temperature of the outgoing atomic beam, a much larger detuning ($\delta \sim -7\Gamma$ for our laser intensity) is preferable.

A pulsed operation of the MM-MOT may provide, for a given application, an output beam with better characteristics than this compromise. First, one loads the MM-MOT with the detuning which maximizes the capture rate R and with a zero launch velocity ($\omega = \omega'$). During this phase of duration t_1 , the number of trapped atoms varies according to $N(t) = (RL/\gamma)(1 - e^{-\gamma t})$. One then switches the detuning of the trapping lasers to a much larger value, with $\omega \neq \omega'$ set to provide the required velocity \bar{v} . This launching phase must last a time $t_2 = (L + D)/\bar{v}$, so that all trapped atoms can leave the MM-MOT and reach the magnetic guide. The optimization of t_1 depends on the relative value of the escape time γ^{-1} and the launching time t_2 . For a low Rb vapor pressure (small R and small γ), the largest flux corresponds to

$$\gamma t_2 \ll 1 \quad : \quad \Phi \simeq RL \quad \text{for} \quad t_1 = \sqrt{2t_2/\gamma}. \quad (6)$$

In this case, the flux Φ in the guide is equal to the capture rate of the MM-MOT and the operation in pulsed mode does not lead to a loss in efficiency. If we increase the Rb vapor pressure in the cell and thus the rate R so that $\gamma \sim t_2^{-1}$, the optimum operation of the pulsed mode corresponds to

$$\gamma t_2 \sim 1 \quad : \quad \Phi \sim 0.3 RL \quad \text{for} \quad t_1 \sim t_2 \sim \gamma^{-1}. \quad (7)$$

This pulsed mode makes the extraction of atoms from the MM-MOT much easier. In the continuous mode, the detuning of the MM-MOT laser beams is relatively small ($\delta \sim -3\Gamma$) so that the outgoing atoms may be deflected or accelerated by the fringe field of the trapping laser beams, as already described. This spurious effect is strongly decreased if the detuning of these lasers is increased to a

value $\delta \sim -7\Gamma$ while the atoms travel in the “dangerous” region.

We note that, as for the continuous mode of operation, the loading of the magnetic guide from the MM-MOT may be improved by an auxiliary 2D MOT located between the exit of the MM-MOT and the guide. Also, although the atomic beam is now pulsed at the entrance of the guide, the pulses broaden as they propagate because of the longitudinal velocity dispersion Δv . This entails that a quasi-continuous beam is obtained after a distance $\sim L\bar{v}/\Delta v$ if one chooses $t_1 \sim t_2$.

3.4 Position and velocity distribution of the guided atoms

We have studied experimentally the various ways for loading the magnetic guide discussed above, *i.e.* without or with the auxiliary 2D MOT, and for a continuous or pulsed operation of the MM-MOT. As for the MM-MOT itself, we have determined the longitudinal and transverse temperatures of the atoms in the guide, as well as the flux of the guided beam.

3.4.1 Longitudinal velocity distribution

The measurement of the longitudinal velocity distribution is quite straightforward if we operate the MM-MOT in pulsed mode, since we can derive the longitudinal temperature directly from the temporal width of the absorption signal when a given atom pulse passes through the probe beam. This beam is located downstream, at 40 cm from the entrance of the magnetic guide. The results are given in Fig. 9, as a function of the detuning δ_2 of the auxiliary MOT. This figure also gives the results obtained in the absence of the auxiliary MOT.

We find that the temperatures are always lower for larger velocities ($\bar{v} = 2.6$ m/s). This is the opposite of what we found just at the output of the MM-MOT. It is probably due to the heating of the atoms by the stray light of the various trapping beams, when they travel over the distance D between the MM-MOT and the guide. This heating is larger if the atoms spend more time in this region, *i.e.* if they are slow. The presence of the auxiliary MOT causes some additional heating of the atomic beam which is also proportional to the time spent by the atoms in the laser beams. For $\delta_2 = -6.5\Gamma$, the increase of the longitudinal temperature of the beam is at most 30%, while, as we shall see, the transverse temperature decreases by an order of magnitude, thanks to the auxiliary MOT.

When the MM-MOT is operated in continuous mode, we found much larger longitudinal temperatures, in the range of 0.5–1 mK. We think that this is due to the acceleration and heating of the atoms when they travel between the MM-MOT and the guide, the heating being much more dramatic than in the pulsed mode, since the trapping beams are much closer to resonance.

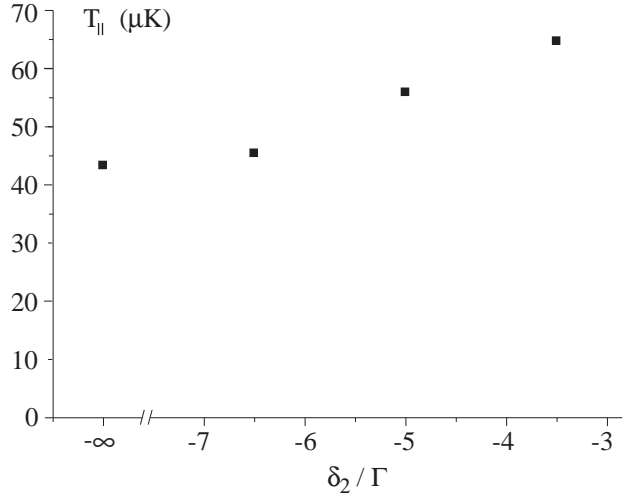


Fig. 9. Longitudinal temperature in the magnetic guide, as a function of the detuning δ_2 of the auxiliary MOT. The value found in absence of the auxiliary MOT, the MM-MOT is operated in pulsed mode with $\bar{v} = 2.6$ m/s, $b' = 1.5$ T/m.

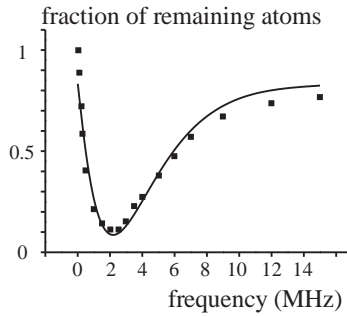


Fig. 10. Fraction of remaining atoms as a function of the radio-frequency applied in a region located between the entrance of the guide and the detection region. From this set of results, we deduce the transverse temperature of the guided atomic beam, here $170\mu\text{K}$. Here the MM-MOT is operated in pulsed mode with $\bar{v} = 2.6$ m/s, $b' = 1.5$ T/m. The detuning of the auxiliary MOT is $\delta_2 = -6.5\Gamma$.

3.4.2 Transverse temperature

The transverse temperature in the guide has been measured in two ways, which give consistent results. First, we can use the method already described for the characterization of the MM-MOT which consists in scanning the position of the probe laser beam, in order to reconstruct the transverse profile of the atomic beam. Alternatively, we can use radio-frequency evaporation to selectively remove a fraction of the atomic distribution. From the variation of the fraction of remaining atoms as a function of the radio-frequency, we can infer the transverse temperature of the atomic beam.

A result obtained with this second method is shown in Fig. 10. It has been obtained with a pulsed loading in presence of the auxiliary MOT. We find that the losses of atoms are maximal for a radio-frequency ~ 2 MHz. Using

a simple numerical model based on a Monte-Carlo sampling of the atomic distribution, we can determine from this set of data the transverse temperature of the beam, which is in this case $\sim 170 \mu\text{K}$.

We have measured the transverse temperature of the magnetically guided atoms in the presence of the auxiliary MOT, using the MM-MOT either in the continuous or the pulsed regime and we have obtained similar results. The variation of the transverse temperature with the magnetic gradient b' and the longitudinal velocity is in good agreement with the prediction (5), where D should be replaced by the distance $D' \sim 4 \text{ mm}$ between the exit of the auxiliary MOT and the entrance of the magnetic guide. We did not find a strong dependence of the transverse temperature of the guided atoms on the detuning δ_2 of the auxiliary 2D-MOT, which can be understood easily. When $|\delta_2| > 5 \Gamma$, one expects transverse temperatures within the 2D MOT in the $10 \mu\text{K}$ range. The corresponding kinetic energy is negligible compared with the energy (5) resulting from the divergence of the atomic beam, as the atoms travel over the distance D' .

In absence of the auxiliary MOT, we have measured much larger transverse temperatures inside the guide, in the range of 1-2 mK. This is a consequence of the increase of the beam's transverse size at the magnetic guide entrance, after free propagation over the distance D . The variation of the transverse temperature with b' and \bar{v} is also in good agreement with the prediction (5).

3.4.3 Flux

The flux of atoms in the magnetic guide is not significantly modified by the presence of the auxiliary MOT. Operating in continuous mode at a pressure $P_{87} = 10^{-8} \text{ mbar}$, we find that this flux varies between $1.5 \cdot 10^8$ and $3 \cdot 10^8$ atoms/s, when \bar{v} varies between 1.5 m/s and 3 m/s. This corresponds to a transfer efficiency between 15% and 30%. Similar values are achieved in pulsed mode if we optimize the loading time t_1 according to (6).

For velocities smaller than 1.5 m/s, we did not find that a significant fraction of the atoms emitted by the MM-MOT could be transferred to the magnetic guide. We attribute this fact to the depletion of the slow atomic beam by collisions with atoms from the rubidium vapor in the cell. The slow atoms have to travel over a distance $\sim 10 \text{ cm}$ through the cell and the tube ensuring the differential pumping, before they arrive in the ultra-high vacuum region of the magnetic guide. For $P_{87} = 10^{-8} \text{ mbar}$ (i.e. a total rubidium pressure $4 \cdot 10^{-8} \text{ mBar}$) and $\bar{v} = 1.5 \text{ m/s}$, we estimate the atomic flux to be reduced by 40 % over this distance. This decay factor is expected to vary as $\exp(-\alpha P_{87}/\bar{v})$ (where α is a numerical constant), which we check experimentally by varying P_{87} between 10^{-9} mbar and 10^{-8} mbar and \bar{v} between 1 m/s and 3 m/s. The decay makes the guided beam very difficult to detect for ultra-low velocities ($\bar{v} \leq 1 \text{ m/s}$), especially if one also takes into account the increase of the transverse temperature for low \bar{v} (see eq. (5)). On the other hand, for relatively large velocities ($\bar{v} \geq 2.5 \text{ m/s}$), the flux of

guided atoms is close to the one expected from a uniform repartition of the atoms among the three possible Zeeman sublevels (the untrapped levels $m = 1, 0$ and the trapped one $m = -1$), *i.e.*, 1/3 of the atoms emerging from the MM-MOT.

4 Conclusion and perspectives

We have presented in this paper the experimental study of the production of a slow atomic beam from a “moving molasses + magneto-optical trap” setup (MM-MOT), and the transfer of this beam into a magnetic guide. This setup can be operated in continuous as well as in pulsed mode. In particular, our results prove that the light scattering from the atoms being captured in the MM-MOT can be kept low enough to avoid perturbations of the propagation of the atoms in the guide. This is a crucial point for future work towards the goal of this project, which consists in performing evaporative cooling in the magnetic guide. Our approach constitutes an alternative to the multiple loading of a 3D magnetic trap [44,45].

Due to the particular geometry of our setup, the best transfer between the MM-MOT and the magnetic guide is ensured by using an auxiliary transverse 2D-MOT which nearly fills the $D = 25 \text{ mm}$ gap between the end of the MM-MOT and the entrance of the magnetic guide. The price to pay for the gain in transverse confinement is a slight increase of the longitudinal temperature of the atoms, due to the recoil heating along the beam axis. This auxiliary 2D-MOT will be unnecessary in the new version of our setup where the distance D will be considerably reduced.

The lowest longitudinal temperature of the guided atoms has been obtained by operating the MM-MOT in pulsed mode, *i.e.* by switching the detuning of the MM-MOT laser beams to a large value (typically seven line widths) during the launching phase. In this way, we can minimize the acceleration of the atoms by the laser stray light as they travel over the distance D . For a longitudinal velocity $\bar{v} = 2 \text{ m/s}$, the measured longitudinal temperature is $\sim 50 \mu\text{K}$. The transverse temperature is significantly larger ($\sim 170 \mu\text{K}$), as a consequence of the divergence of the atomic beam between the exit of the MOT region and the entrance of the magnetic guide. The transverse spatial spreading of the atomic beam translates into an increase of the transverse temperature, as expressed by (5).

The largest atom flux in the guide is $\sim 3 \cdot 10^8$ atoms/s, and it is limited by the loading flux of the MM-MOT, which is itself proportional to the ^{87}Rb vapor pressure in the cell. Going to higher pressures would improve the loading flux, but it would also increase the collisional losses of the slow atomic beam on its way to the magnetic guide. A decisive improvement in this context is to turn to a MM-MOT loaded from an auxiliary slow atomic beam. This increases the complexity of the setup, but should allow for a ten times larger guided flux.

The continuous operation of our setup is in contrast with the pulsed loading of a magnetic guide as reported

in [17]. In that work, 10^5 atoms were coupled into a four-wire guide from a 3D-MOT, whereas the pulsed operation of our present system gives up to 10^7 atoms/cycle, with comparable longitudinal and transverse temperatures.

Finally, we note that the collision rate on axis in our setup, which scales as $\Phi/(\bar{v}T)$, is at present $\sim 3 \cdot 10^{-2} \text{ s}^{-1}$. This is still much too small to initiate evaporative cooling. However, we expect to increase the flux by a factor 10 using an auxiliary slow atomic beam. Another factor 10 should be gained from an improved transfer scheme from the MM-MOT into the magnetic guide, since this will decrease the temperature T of the trapped atoms and allow to work at a lower average velocity \bar{v} . In these conditions, an adiabatic compression of the atomic beam within the guide, using for instance permanent magnets, should lead to a collision rate in the usual range for compressed magnetic traps, compatible with a spatial evaporation along a guide of reasonable length.

C. F. Roos acknowledges support from the European Union (contract HPMFCT-2000-00478). A. Aclan was supported by a grant from Volkswagen and the Gottlieb Daimler and Karl Benz-Stiftung. This work was partially supported by CNRS, the Région Ile-de-France, Collège de France and DRED.

References

1. S. Chu, Rev. Mod. Phys. **70**, 685 (1998).
2. C. Cohen-Tannoudji, Rev. Mod. Phys. **70**, 707 (1998).
3. W.D. Phillips, Rev. Mod. Phys. **70**, 721 (1998).
4. A. Fioretti, D. Comparat, A. Crubellier, O. Dulieu, F. Masnou-Seeuws, and P. Pillet, Phys. Rev. Lett. **80**, 4402 (1998).
5. T. Takekoshi, B. M. Patterson, and R. J. Knize, Phys. Rev. Lett. **81**, 5105 (1998).
6. J. Weinstein, R. deCarvalho, T. Guillet, B. Friedrich, and J. Doyle, Nature **395**, 148 (1998).
7. H. L. Bethlem, G. Berden, F. M. H. Crompvoets, R. T. Jongma, A. J. A. van Roij, and G. Meijer, Nature **406**, 491 (2000).
8. For a review, see e.g. *Special Issue on Atom Optics and Interferometry*, A. Aspect and J. Dalibard eds, C. R. Acad. Sci. Paris, t. 2, Série IV, N°4;
9. See e.g. G. Santarelli *et al.*, Phys. Rev. Lett. **82**, 4619 (1999) and refs. in.
10. For a review, see e.g. *Bose-Einstein Condensation in Atomic Gases*, Proceedings of the International School of Physics "Enrico Fermi", eds M. Inguscio, S. Stringari, and C. Wieman (IOS Press, 1999).
11. E. Mandonnet, A. Minguzzi, R. Dum, I. Carusotto, Y. Castin and J. Dalibard, Eur. Phys. J. D **10**, 9 (2000).
12. J. Schmiedmayer, Phys. Rev. A **52**, R13-R16 (1995).
13. J. Denschlag, D. Cassettari, and J. Schmiedmayer, Phys. Rev. Lett. **82**, 2014 (1999)
14. A. Goepfert, F. Lison, R. Schütze, R. Wynands, D. Haubrich, and D. Meschede, Appl. Phys. B **69**, 217 (1999)
15. M. Key, I. G. Hughes, W. Rooijakkers, B.E. Sauer and E.A. Hinds, D.J. Richardson and P.G. Kazansky, Phys. Rev. Lett. **84**, 1371 (2000)
16. N. H. Dekker, C. S. Lee, V. Lorent, J. H. Thywissen, S. P. Smith, M. Drndic, R. M. Westervelt, and M. Prentiss, Phys. Rev. Lett. **84**, 1124 (2000)
17. B.K. Teo and G. Raithel, Phys. Rev. A **63**, 031402 (2001).
18. J. A. Sauer, M. D. Barrett, and M. S. Chapman, Phys. Rev. Lett. **87**, 270401 (2001)
19. E.A. Hinds and I.G. Hughes, J. Phys. D: Appl. Phys. **87**, R119, (1999).
20. J.V. Prodan, W.D. Phillips and H. Metcalf, Phys. Rev. Lett **49**, 1149 (1982).
21. W. Ertmer, R. Blatt, H. Hall and M. Zhu, Phys. Rev. Lett **54**, 996 (1985).
22. E. Riis, D. Weiss, K. Moler, and S. Chu, Phys. Rev. Lett. **64**, 1658 (1990).
23. J. Nelessen, J. Werner, and W. Ertmer, Opt. Commun. **78**, 300 (1990).
24. T. Swanson, N. Silva, S. Mayer, J. Maki, and D. McIntyre, J. Opt. Soc. Am. B **13**, 1833 (1996).
25. F. Lison, P. Schuh, D. Haubrich and D. Meschede, Phys. Rev. A **61**, 013405 (1999).
26. H. Chen and E. Riis, Appl. Phys. B **70**, 665 (2000).
27. K. Dieckmann, R. J. C. Spreeuw, M. Weidemüller and J. T. M. Walraven, Phys. Rev. A **58**, 3891 (1998).
28. J. Schoser, A. Batär, R. Löw, V. Schweikhard, A. Grabowski, Yu. B. Ovchinnikov and T. Pfau, physics/0201034
29. S. Weyers, E. Aucouturier, C. Valentin and N. Dimarcq, Opt. Commun. **143**, 30 (1997).
30. G. Duddle, N. Sagna, P. Berthoud and P. Thomann, J Phys. B: At. Mol. Opt. Phys. **29**, 4659 (1996).
31. P. Berthoud, A. Joyet, G. Dudle, N. Sagna and P. Thomann, Europhys. Lett. **41**, 141 (1998).
32. Z.T. Lu, K.L. Corwin, M.J. Renn, M.H. Anderson, E.A. Cornell and C.E. Wieman, Phys. Rev. Lett. **77**, 3331 (1996).
33. K. I. Lee, J. A. Kim, H. R. Noh, and W. Jhe, Opt. Lett. **21**, 1177 (1996).
34. R. S. Williamson III, P. A. Voytas, R. T. Newell and T. Walker, Optics Express **3**, 3, 111 (1998).
35. J.J. Arlt, O. Marago, S. Webster, S. Hopkins and C.J. Foot, Opt. Commun. **157**, 303 (1998).
36. W. Wohlleben, F. Chevy, K. Madison, and J. Dalibard, Eur. Phys. J. D **15**, 237 (2001).
37. L. Cacciapuoti, A. Castrillo, M. de Angelis and G.M. Tino, Eur. Phys. J. D **15**, 245 (2001).
38. G. Grynberg, B. Lounis, P. Verkerk, J.Y. Courtois, and C. Salomon, Phys. Rev. Lett. **70**, 2249 (1993).
39. F. Reif, *Fundamentals of statistical and thermal physics* (McGraw-Hill, New York, 1965).
40. D.S. Weiss, E. Riis, Y. Shevy, P.J. Ungar and S.Chu, J. Opt. Soc. Am. B **6**, 2072 (1989).
41. C. Salomon, J. Dalibard, W.D. Phillips, A. Clairon and S. Guelatti, Europhys. Lett. **12**, 683 (1990).
42. L. D. Landau and E. M. Lifshitz, Quantum Mechanics, §90, Pergamon Press, Oxford (1977).
43. N. V. Vitanov and K.-A. Suominen, Phys. Rev. A **56**, R4377 (1997).
44. E. A. Cornell, C. Monroe, and C. E. Wieman, Phys. Rev. Lett. **67**, 2439 (1991).
45. H. J. Davies and C. S. Adams, J. Phys. B: At. Mol. Opt. Phys. **33**, 4079, (2000).